PHYSICAL REVIEW B VOLUME 53, NUMBER 8 15 FEBRUARY 1996-II

Solid-phase epitaxy induced by low-power pulsed-laser annealing of III-V compound semiconductors

G. Vitali, L. Palumbo, M. Rossi, G. Zollo, and C. Pizzuto
Dipartimento di Energetica, Università La Sapienza and Instituto Nazionale di Fisica della Materia,
Via A. Scarpa 14, 00161 Rome, Italy

L. Di Gaspare and F. Evangelisti
Dipartimento di Fisica, III Università di Roma and Istituto Nazionale di Fisica della Materia, P. A. Moro 5, 00185 Rome, Italy

(Received 25 July 1995; revised manuscript received 2 November 1995)

Low-power pulsed-laser annealing (LPPLA) was applied to III-V compound semiconductors GaAs and InP. The effects have been analyzed using several experimental techniques such as reflection high-energy electron diffraction, Rutherford backscattering spectroscopy, x-ray photoelectron spectroscopy, and electrical measurements. In addition, a calculation method was developed to study the heat propagation in the irradiated sample during the LPPLA process. The irradiation conditions, realizing a uniform surface laser-energy distribution, made possible a unidimensional approach. The results obtained experimentally and by numerical modeling agree well if one assumes that a solid-phase epitaxy takes place. The XPS measurements for GaAs and InP show, in particular, that a range of the irradiation power density exists where the LPPLA can effectively restore the lattice order without appreciable alteration of the surface stoichiometry. At higher power density of irradiation, the As and P vacancies introduced by the laser, in GaAs and InP, respectively, may no longer be neglected.

I. INTRODUCTION

It is well known that ion implantation is nowadays the most reliable doping techniques for III-V semiconductor materials.[1,2] The main reasons for this lie in the shortcomings of the conventional thermal diffusion technique, namely the poor control of the doping profile and the stoichiometric instability of the surface. The high temperatures T requested to induce an efficient diffusion processing can often exceed the critical temperature T_c, characteristics of the material. On definition, at $T>T_c$ the alteration of the stoichiometry due to different thermal volatility of the components can no longer be neglected,[3–6] typical values being $T_c \cong 600$ °C for GaAs,[5] and $T_c \cong 300$ °C for InP.[6] On the other hand, ion implantation, considered generally as a low-temperature technology, requires a recovery of the structural damage produced by the bombarding ions and activation of the electrical carriers. Conventional annealing normally increases the specimen temperature above the critical value T_c (Refs. 7–9) so that one of the two components begins to sublimate at a higher rate, leaving many vacancies in the substrate. To overcome this complication, one has to heat the specimens in an overpressure of the more volatile component or alternatively to use specimen capping. Even if all the processing regimes were well established, their application would add substantial additional costs to the devices based on III-V compounds which would overshadow the merits of their advanced performance, e.g., high electron mobility, etc. It would make a difference, however, if one could anneal the specimen in the implantation chamber, and so avoid specimen contamination during transportation or use of additional precautions.

One of the first attempts in this direction was to make use of conventional high-power lasers. At this kind of annealing, however, the recovery of the implanted region to a single-crystal state occurs from a melted material.[10] Equally unsuccessful was the use of low-power annealing by continuous-wave lasers, which also results in heating up to high temperatures. As a consequence, the application of these two techniques to compound semiconductors like GaAs and InP does not successfully resolve the problem related to the alteration of the surface stoichiometry.

An alternative technique called low-power pulsed-laser annealing (LPPLA) (Ref. 7) was demonstrated[11,12] to remove the damage introduced by ion implantation at temperatures much below the melting. It was shown[12] that in this case the experimental condition required to recover the upper layers of GaAs and InP samples without decomposition of the stoichiometry is to keep its temperature $T<T_c$ strictly at any point of the irradiated surface.[11,13] This can be achieved by using an optical homogenizer, which is able to ensure uniform intensity of the laser pulse across the beam. As a consequence the lateral heat flow (along the surface) can be neglected, and the presence of transversal temperature gradients will depend on the intrinsic characteristics of the implanted material only, i.e., on inhomogeneous absorption coefficients rather than on a not-uniform lateral distribution of the energy. One can therefore consider the laser effects to be caused by a uniform (in a well-determined time interval) two-dimensional heat source that varies only with the in-depth coordinate due to the light absorption of the material.

In the present paper we present experimental and numerical data on applying LPPLA in the conditions outlined above to two III-V compound semiconductors: GaAs and InP. Both materials are ideal candidates for LPPLA since each one contains a component with sublimation temperature far below the melting point of the compound and therefore the condition $T<T_c$ is crucial.

Experimental results on the effects of LPPLA and the cor-

0163-1829/96/53(8)/4757(13)/$06.00

© 1996 The American Physical Society

TABLE I. Implantation conditions for GaAs and InP specimens.

	Implanted ion	Dose (atoms/cm^2)	Energy (keV)	Temperature (°C)	R_p (nm)	ΔR_p (nm)
GaAs	Zn^+	10^{14}	140	110±10	56.6	27.8
InP	Zn^+	10^{14}	140	110±10	75.2	39.5

responding observation technique used include (a) structural reordering of the ion-induced defects studied by reflection high-energy electron diffraction (RHEED) and Rutherford backscattering (RBS) analysis; (b) activation of the electrical carriers demonstrated by electrical measurements; and (c) evaluation of the As/Ga ratio near the surface of laser-beam-treated GaAs, based on x-ray photoelectron spectroscopy (XPS) analysis.

A complementary mathematical model is developed to predict the laser-induced heat distribution in GaAs and InP samples up to temperatures corresponding to the critical value T_c defined above. The model is based on the assumption that the laser energy absorbed in the material is instantaneously transferred into a lattice as heat source. This implies that the real temperature rise in the specimen should, in any case, not exceed the calculated one. A detailed comparison of the limits of the theoretical calculations and the experimental results is discussed.

Since the temperature range of interest is far below the melting point of the materials considered, the recovery of the crystalline order cannot be attributed to a local melting of the specimen (as in the high-power pulsed-laser annealing, HPPLA). The process is discussed in terms of a solid-phase epitaxial regrowth instead.

II. EXPERIMENTAL

A. Ion implantation

The specimens used in the annealing experiments were (100) single-crystals wafers of semi-insulating GaAs and InP (Sumitomo Corporation Ltd., Japan). They were implanted in a random direction at 7° tilt, with Zn ions, at an energy of 140 keV and a dose of 10^{14} cm^{-2}. The ion current did not exceed 2 μA cm^{-2}, and during the implantation process the samples were intentionally heated at 110±10 °C. The implantation conditions, together with the obtained projected range and straggling, are reported in Table I.

B. LPPLA (low-power pulsed-laser annealing)

The LPPLA experiments were carried out directly in air at room temperature, irradiating the ion-implanted samples with a *Q*-switched Standard Ruby Laser System (JK model 3330). A homogeneous energy distribution across the beam was achieved by using an optical system consisting of a condenser and an optical guide. This ensures a mixing of the radiation spatial modes which results in losing the spatial coherence, and then in a homogenization of the energy across the beam.[12,14]

The number of laser pulses was varied between 10 and 30, the duration of each pulse being $\Delta t_{\mathrm{FWHM}}=25$ ns. The mean power density P_0 of the pulse, defined as the energy of the pulse divided by Δt_{FWHM}, was varied between 4.5 and 7.5 MW/cm^2. After good mechanical, optical, and thermal stabilization of the laser system, it is possible to obtain a pulse-to-pulse amplitude fluctuation in the range of ±2%. The maximum value of the irradiation power density used has been chosen in order to keep the maximum surface temperature of the irradiated sample well below the melting threshold. In our case, indeed, the ion implantation damage being not so heavy to produce amorphization (and, as a consequence, a lower absorption coefficient), the melting occurs with an estimated irradiation power density of about 11 MW/cm^2 (0.275 mJ/cm^2). This evaluation has been obtained by the analytical-iterative method whose details are described in the present paper (see Sec. III A). The pulses repetition rate was about 0.05 Hz and, as a consequence, the time interval between the pulses was so long that the temperature peak caused by each pulse can be considered as starting from the room temperature. The light-absorption depth is larger than the projected range of the implanted ions. All the irradiation conditions and the optical constants are reported in Table II.

C. Analysis techniques

1. RHEED (Reflection high-energy electron diffraction) analysis

The crystal structure of the samples, before and after the annealing, was controlled in a AEI EM6G electron microscope equipped with a high-resolution electron-diffraction stage. Thus it allows the sample rotation around the normal to the surface and, as a consequence, the observation of reflection diffraction patterns corresponding to different azimuthal directions. Moreover, by varying the glancing angle

TABLE II. Optical constants and laser-pulse parameters for GaAs and InP specimens at the ruby wavelength ($\lambda=694.3$ nm).

	Energy laser densities (mJ/cm^2)	Pulse duration (ns)	FWHM (ns)	Reflectivity %	Absorption coeff. (cm^{-1})
GaAs	125–188	56	25	34	28 900
InP	150–175	56	25	30.7	42 350

of the electrons incidence, it was possible to obtain structural information related to different depths of the examined material.

2. RBS (Rutherford backscattering spectroscopy) analysis

The GaAs samples were analyzed by using 1.5- and 2-MeV He^+ ions incident normally onto the specimen surface. The backscattered ions were collected at a scattering angle of $\psi=160°$ and 97°, correspondingly, the analyzer channel width being 5.0 $\mathrm{keV\,ch}^{-1}$. In the case of InP the initial He^+ energy was 1.5 MeV, the scattering angle was 160°, and the detector sensitivity was 3.153 $\mathrm{keV\,ch}^{-1}$.

3. XPS (X-ray photoelectron spectroscopy)

The measurements were performed in an UHV chamber using a monochromatized Al $K\alpha$ photon source ($h\nu=1486$ eV), and a hemispherical electron energy analyzer, the system resolution being 0.35 eV. In order to obtain the largest XPS sampling depth, we have investigated the $3d$ core levels of both Ga and As, i.e., the core levels at lower binding energy of the samples. In these conditions, due to the large escape depth (26 Å) of the emitted photoelectrons with a kinetic energy of about 1450 eV, we have an XPS sampling depth of about 50 Å.[15]

The surface ratio between As and Ga has been determined from the analysis of the As $3d$ core-level densities. To include the effect of the different oxidation of the samples, the As/Ga ratios have been calculated using the integrated XPS intensity, employing as sensitivity factors the 0.025 b/atom for the As $3d$ core level and the 0.014 b/atom for the Ga $3d$ core level, respectively.[16]

4. Electrical measurements

The sheet resistivity measurements were carried out by using the Van der Pauw (VdP) method. In our case the current source and the voltage meter were integrated in a single instrument (Keithley 236). The commutations between the typical configurations of the VdP method were realized using a manual commutator.

III. MODELING OF LLPLA

A. Analytical model

Since the lateral dimensions of the irradiated samples were smaller than the laser beam diameter, and because of the power density uniformity across the beam, we can consider the heat diffusion one-dimensional problem. Furthermore, based on the fact that the thermalization rate of the photoinduced electron-hole pairs is very high (the thermalization time is approximately 10^{-12} s), and that the high density of defects in the implanted region enhances the nonradiative recombination, we assume that the absorbed laser energy is instantaneously transferred into the lattice as thermal energy.

A simple approach consists of solving the linear heat-transfer equation in a double-layer medium where the first layer ($x\in[-l,0]$) is the implanted one, and the second layer $[x\in(0,\infty)]$ is the virgin material. Then the equation describing the temperature T as a function of the position x and time t can be stated as

$$K_{1,2}\,\frac{\partial^2 T}{\partial x^2}+F(x,t)=c_{1,2}\rho_{1,2}\,\frac{\partial T}{\partial t} \tag{1}$$

with the initial condition

$$T(x,t=0)=300\ \ \mathrm{K} \tag{2}$$

and the boundary condition

$$K_1\left(\frac{\partial T}{\partial x}\right)_{x=-l}=0. \tag{3}$$

Here $K_{1,2}$, $c_{1,2}$, and $\rho_{1,2}$ respectively, are the thermal conductivity, the heat capacity, and the density in layer 1 or 2. The source term $F(x,t)$ is linked to the power density $I_0(t)$ of the beam hitting the surface of the sample by the relation

$$F(x,t)=(1-R)I_0(t)\alpha e^{(-\alpha x)}, \tag{4}$$

R and α being respectively the reflection and the absorption coefficients at the ruby wavelength ($\lambda=694.3$ nm). For the beam intensity, on the basis of the revealed wave shape, we assume the following expression:

$$I_0(t)=\begin{cases} a\,\dfrac{e^{-(t-t_0)^2/2b^2}}{b\sqrt{2\pi}}-c, & 0\leqslant t\leqslant 2t_0,\\ 0 & \text{elsewhere,}\end{cases} \tag{5}$$

where a, b, and c assume different values depending on the energy density hitting the sample, and the center of the Gaussian-like pulse shape is placed exactly at $t_0=\frac{1}{2}$ of the laser pulse duration (see Table II, $t_0=28$ ns).

The adiabatic boundary condition can be defined if one considers that the influence of the Stephan-Boltzmann thermal surface radiation on the temperature always remains below 0.12%, so that the heat loss through the specimen surface can be neglected.[17] An additional condition is given by the continuity of the temperature and of the heat flux at the interface, namely

$$T_1(x=0,t)=T_2(x=0,t), \tag{6}$$

$$K_1\left.\frac{\partial T_1}{\partial x}\right|_{(x=0)}=K_2\left.\frac{\partial T_2}{\partial x}\right|_{(x=0)}. \tag{7}$$

The mathematical problem has been solved using the Green-function method,[18–20] which allows us to calculate the temperature distribution induced by an ideal impulsive heat source located at any position inside the sample by means of four thermal functions $G_{i,j}(x,\xi,t)$, as reported in Appendix A.

The general expressions for the temperatures in both the implanted $(i=1)$ and the virgin $(i=2)$ zones, therefore are

TABLE III. Thermal parameters for GaAs and InP specimens (300 K).

	$K_2=K_{\mathrm{cr}}$ [W/(cm K)]	$K_1=K_{\mathrm{impl}}$ [W/(cm K)]	c [J/(g K)]	ρ (g/cm^3)
GaAs	0.5795	3×10^{-2}	0.3287	5.319
InP	0.7395	3.75×10^{-2}	1.325	4.79

$$T_i(x,t)=\int_{-l}^{0} G_{1i}(x,\xi,t)\varphi_1(\xi)d\xi+\int_0^{\infty} G_{2i}(x,\xi,t)\varphi_2(\xi)d\xi-a_i^2\int_0^t G_{1i}(x,-l,t-\tau)\psi(\tau)d\tau$$

$$+\int_0^t\int_{-l}^{0} G_{1i}(x,\xi,t-\tau)f_1(\xi,\tau)d\xi\, d\tau+\int_0^t\int_0^{\infty} G_{2i}(x,\xi,t-\tau)f_2(\xi,\tau)d\xi\, d\tau \qquad (8)$$

$f_i(x,t)=[F_i(x,t)]/c_i\rho_i$ being the source term, $\varphi_i(x)=300$ K the initial condition, a_i^2 the thermal diffusivity in the layer i ($i=1$ and 2) and $\psi(t)=[\partial T_1(x,t)/\partial x]_{x=-l}=0$ K cm^{-1} the adiabatic boundary condition at the surface $x=-l$.

By integration of (8) we obtain $T(x,t)$ representing the time evolution of the in-depth temperature profile in different conditions. Values of the physical parameters of virgin and implanted GaAs and InP needed to calculate the profiles in these materials are listed in Tables II and III.[21,22]

It should be noted that for the implanted layer density and heat capacity we have chosen the same values as for the virgin layer, the main reason being the lack of measurement data in the literature. In any case, it is reasonable to consider that the density of the low-dose-implanted layer does not differ significantly from the virgin material. Furthermore, implantation of such doses at elevated temperature (such as 110 °C) is accompanied by relatively low crystalline disorder, so that an assumption of unchanged heat capacity sounds reasonable.

The above-described formulas have been applied to calculate the temperature behavior of GaAs and InP samples during the laser irradiation at a power density of 5 (Fig. 1) and 6.5 MW/cm^2 (Fig. 2), respectively. The P_0 values used are chosen within the power density intervals (for GaAs and InP) where the LPPLA technique is effective. The results of the calculations clearly show that, in any case, the obtained temperatures are quite below the melting point. Furthermore, the respective maximum surface temperature are 728 K for GaAs irradiated at 5 MW/cm^2 (Fig. 1), and 687 K for InP irradiated at 6.5 MW cm^2 (Fig. 2). These results indicate that, at the above-specified irradiation conditions, InP reaches temperatures above its critical temperature (about 300 °C) while GaAs does not exceed its critical temperature T_c (about 600 °C). While the calculation for GaAs agree with the experimental results (see RHEED, XPS, and RBS data), indicating that GaAs irradiation with 5 MW/cm^2 does not cause exceeding of the stoichiometric alteration limit (600 °C), the results obtained for the analytical calculation for 6.5-MW/cm^2-irradiated InP seem to be in contrast with the experimental results (see RHEED, XPS, etc.).

In order to estimate the accuracy of the two-layer model in evaluating the maximum surface temperature reached during laser irradiation, we compare (for the GaAs case) the surface temperature behavior obtained with this analytical model and a more realistic numerical method outlined in Sec. III B. As can be seen in Fig. 3, where the results of the

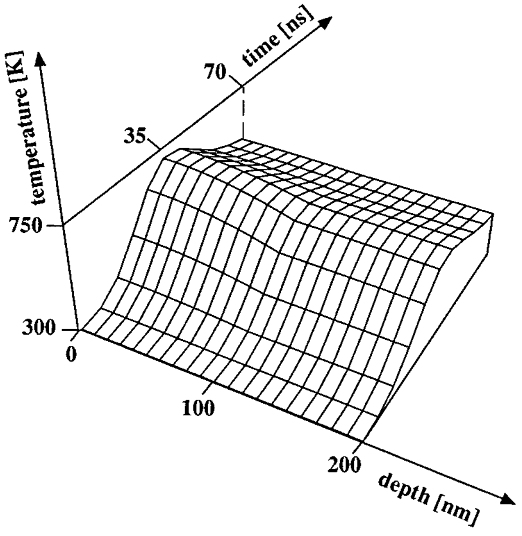

FIG. 1. Analytical calculations of the temperature distribution as a function of the time and the depth inside the sample for a GaAs-irradiated sample with a power density of 5 MW/cm^2.

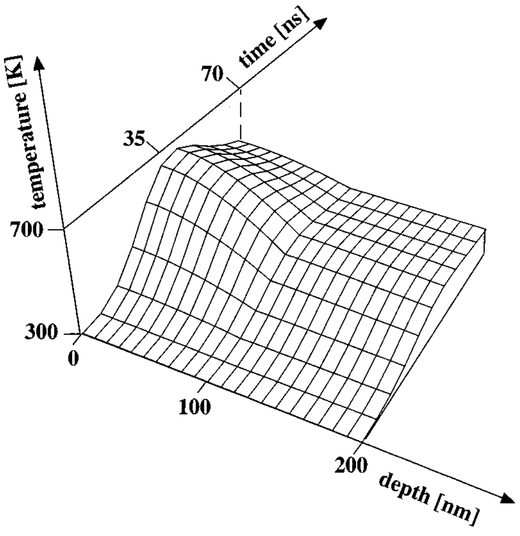

FIG. 2. Analytical calculations of the temperature behavior as a function of the time and depth inside the sample for an InP-irradiated sample with a power density of 6.5 MW/cm^2.

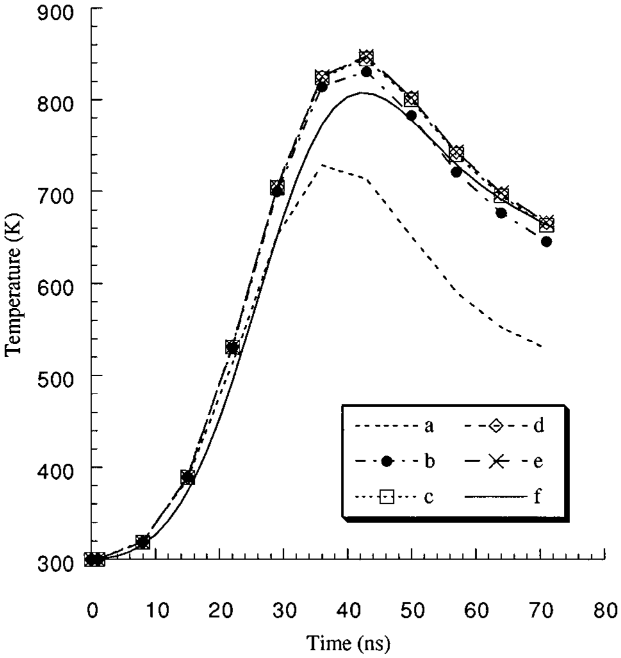

FIG. 3. Comparison between the surface temperatures during the irradiation at 5 MW/cm^2 of a GaAs sample, calculated by the analytical model in an iterative way, using constant thermal parameters at 300 (curve *a*), 730 (curve *b*), 831 (curve *c*), 845 (curve *d*), and 847 K (curve *e*), and by the numerical model (curve *f*).

comparison are presented, the analytical prediction (curve *a*), is considerably below the numerical calculation (curve *f*), the deviation parameter

$$\frac{\Delta T}{T}\times 100=\frac{T_{\text{num}}-T_{\text{an}}}{T_{\text{num}}}\times 100 \tag{9}$$

being of the order of 9.8%. T_{num} and T_{an}, respectively, are the numerical and the analytical maximum temperatures.

This comparison shows that the analytical model can only be considered an approximation of the "real" maximum surface temperature value, i.e., for a rough estimation of how far is the temperature reached from the melting point. In order to decrease the deviation parameter, we used an iteration step procedure. That is at each step of the analytical calculation the surface temperature was evaluated by using constant thermal parameters estimated at the maximum surface temperature reached in the preceding step. These results are also reported in Fig. 3 (curves *b*–*e*), and demonstrate that the iteration data rapidly converge, slightly overestimating the maximum temperature reached (at a given *t*) in the numerical calculation. This behavior is due to the decrease of the Green-function prime derivative with respect to the temperature down to values practically negligible with increasing the temperature and time. The temperature deviation parameter decreases down to about 5%.

B. Numerical model

The assumption of constant thermal parameters within the frames of the double-layer model have allowed us to solve the exposed heat-propagation problem analytically. This simple solution gives valuable rough estimates of surface temperature to prevent melting of the material under irradiation.

The model is not quite suitable, however, for ion-implanted specimens, since the ion-induced damage is distributed inside the substrate and a multilayer model would be therefore a better approximation.[23] Indeed, to obtain more accurate information on the upper limits of the laser power density where the substrate stoichiometry begins to alter, and to define the corresponding temperature energy distribution during the irradiation, it is necessary to take into account the inhomogeneity of the ion-implanted specimen and the nonlinear temperature dependence of the thermal parameters $K(T)$, $c(T)$, and $\rho(T)$, according to the summary in Table IV.[21,22] Hence a more realistic approach to the problem needs the solution of nonlinear inhomogeneous heat-transfer equation in an inhomogeneous medium:

$$\frac{\partial}{\partial x}\left(K(x,T)\frac{\partial T}{\partial x}\right)+F(x,t)=c(x,T)\rho(x,T)\frac{\partial T}{\partial t}. \tag{10}$$

The complexity of the nonlinearity in such a medium requires a numerical approach to be used. We first need to define a model for the inhomogeneity of the ion-implantation-induced damaging of the specimen. The analysis of this damage in the implantation conditions used shows that the damage distribution is similar to the Gaussian-like distribution of the implanted impurities.[24] The maximum of the damage distribution can slightly differ (usually by up to 10%) from that of the implanted species, its position depending on the ion mass and energy. At a first approximation, we will assume that the centers of the damage and implanted-ion distributions are located at the same depth. Furthermore, since the high-resolution transmission electron microscopy (HRTEM) analysis of implanted specimens indicates that the damaging consists of clusters of defective material dispersed in a crystalline matrix,[25] it appears reasonable to consider the macroscopical thermal conductivity as a Gaussian function of the in-depth coordinate with a minimum centered at the maximum damage.

That is, we can define

TABLE IV. Temperature dependence of GaAs and InP thermal parameters.

	$K_{\text{cr}}(T)$ [W/(cm K)]	$K_{\text{impl}}(T)$ [W/(cm K)]	$c(T)$ [J/(g K)]	$\rho(T)$ [g/cm^2]
GaAs	$\frac{544}{T^{1.2}}$	3×10^{-2}	$0.307+7.25\times 10^{-5}T$	$5.319-(T-300)\times 10^{-4}$
InP	$\frac{289}{T^{1.45}}$	3.75×10^{-2}	$0.64+0.228\times 10^{-2}T$	4.79

$$K(x,T)=K_{\mathrm{cr}}(T)-[K_{\mathrm{cr}}(T)-K_{\mathrm{impl}}(T)]\exp\left(-\frac{(x-R_p)^2}{2\Delta R_p^2}\right) \tag{11}$$

where the functions $K_{\mathrm{cr}}(T)$ and $K_{\mathrm{imp}}(T)$, reported in Table IV, are the heat conductivity of the crystalline material $[K_{\mathrm{cr}}(T)]$ and the maximum damage layer $[K_{\mathrm{impl}}(T)]$, respectively, R_p and ΔR_p are the mean implanted-ion range and range straggling, respectively.

The problem has been solved using a finite-difference method stable in the time and space scales, with respect to the temperature variation involved in the LPPLA of implanted specimens. A simple explicit finite-difference scheme is stable if:[26–29]

$$\tau \leqslant \frac{1}{2}\frac{h^2}{a^2}, \tag{12}$$

where τ and h, respectively, are the time and space steps of the bidimensional grid, while a^2 is the thermal diffusivity. As a consequence it cannot be used when the requested time step and the minimum space step are 10^{-9} s and 5×10^{-9} m, respectively, as in the present case.

For this reason, we adapted the Crank–Nicolson scheme,[26,28,29] which is an implicit unconditionally stable method, to the nonuniform grid obtained, gradually refining the space step near the maximum of the damage distribution. The numerical scheme is developed starting from the equation

$$\begin{aligned}\frac{\partial^2 T}{\partial x^2} &= \Psi(x,t,T,T_x,T_t)\\ &= -\frac{F(x,t)}{K(x,T)}+\frac{c(x,T)\rho(x,T)}{K(x,T)}\frac{\partial T}{\partial t}\\ &\quad -\frac{\partial T}{\partial x}\left(\left.\frac{\partial \ln[K(x,T)]}{\partial x}\right|_{T=\mathrm{cost}}\right.\\ &\quad \left.+\frac{\partial T}{\partial x}\left.\frac{\partial \ln[K(x,T)]}{\partial T}\right|_{x=\mathrm{cost}}\right).\end{aligned} \tag{13}$$

Using the finite difference operators involved in the Crank-Nicolson scheme,[26,28,29] we first obtained a nonlinear algebraic equations system which can be reduced to a linear one as shown in Appendix B. The obtained linear algebraic equations system, reduced in tridiagonal form, has been solved using an iterative algorithm[26,27] in the FORTRAN code. The obtained data were processed to yield three-dimensional plots of the temperature over time and depth coordinates representing the time evolution of the in-depth temperature profile during the laser irradiation.

IV. RESULTS AND DISCUSSION

A. GaAs case

We will first discuss the application of the methods outlined above to the laser irradiation of implanted GaAs specimens. The implantation conditions are specified in Table I. Figure 4 illustrates the expected temperature behavior of GaAs samples following their implantation and treatment with a laser pulse of $P_0=5$ MW/cm^2 (i.e., an energy density of 125 mJ/cm^2). One can note that under these conditions the laser pulse will cause a maximum temperature of about 807 K at the surface, which appears 42 ns after the beginning of the pulse. This value is well below the critical dissociation temperature $T_c=873$ K, at which the As evaporation rate is no more negligible.[6]

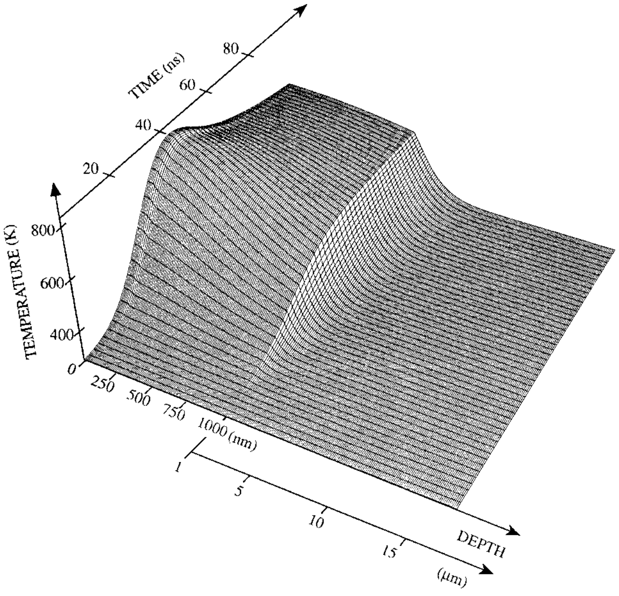

FIG. 4. Temperature distribution, calculated by the numerical model, in a GaAs sample irradiated with a power density of 5 MW/cm^2 as a function of depth and time (Ref. 13).

1. RHEED analysis

The RHEED pattern analysis of the virgin and annealed GaAs specimens [Figs. 5(a)–5(c)] shows that the irradiation with 30 pulses of 5 MW/cm^2 supplies sufficient energy to recover the crystalline order without concurrent stoichiometric changes due to the cumulative losses of As atoms: in

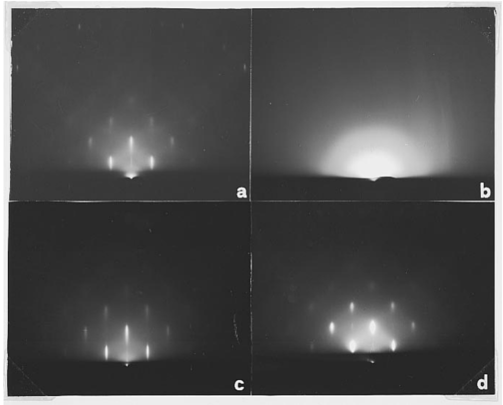

FIG. 5. Diffraction patterns along the ⟨001⟩ azimuthal direction of GaAs samples virgin (a), implanted (b), and laser annealed with 30 pulses of power density 5 (c), and 6 MW/cm^2 (d).

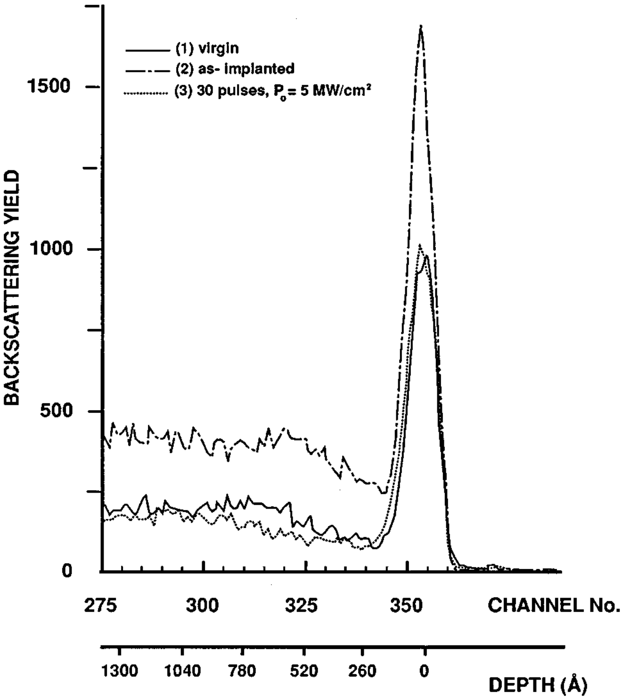

FIG. 6. Rutherford backscattering spectra of GaAs samples in the channeling mode: virgin (1), as-implanted (2), and implanted plus LPPLA with 30×5 MW/cm^2 (3); 2 MeV He$^+$ scattering angle 150° (Ref. 12).

fact the diffraction pattern of the laser-annealed specimen [Fig. 5(c)] appears quite regular in the geometry, and the spots have a narrow bar form, in agreement with the calculations prediction.

2. *RBS analysis*

In Fig. 6 we compare the aligned spectra obtained for virgin, as-implanted, and annealed ($P_0=5$ MW/cm^2) samples. According to the calculations, by irradiating with such a power density, the specimen temperature should rise up to values at which the As-atom losses can still be neglected. From the figure, one can observe that after the LPPLA treatment the surface damage of the implanted sample is about as low as for the virgin specimen, in agreement with the RHEED patterns presented earlier [Figs. 5(a)–5(c)].

3. *XPS analysis*

In order to estimate the behavior of the As atoms in different annealing conditions, we have measured the As/Ga ratio near the surface of the virgin, as-implanted, and annealed samples at LPPLA power density varying from 4.5 up to 7.5 MW/cm^2 with intervals of 0.5 MW/cm^2.

As in the experiments reported in previous sections, the laser treatment was applied in air at room temperature. Obviously the formation of oxides during this irradiation will complicate the analysis itself, and for that reason the XPS analysis was carried out twice, before and after a deoxidization of the specimens using chemical etching in HCl diluted at 3%. As a result we want to eliminate the contribution of the oxides and determine their role. In the case in which it clearly appears that the oxide formation will constitute a limitation for the annealing process, we will have to repeat the treatment in a vacuum chamber or, better, in a controlled atmosphere.

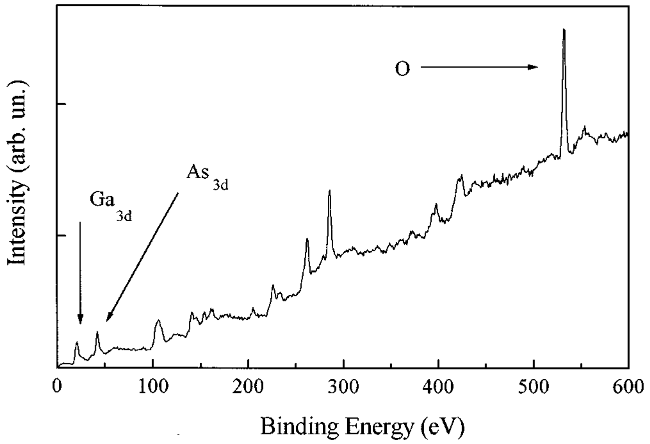

FIG. 7. XPS spectrum of virgin and deoxidized GaAs samples in which are indicated the Ga and As 3*d* levels.

Figure 7 illustrates the full XPS spectrum which was obtained on the GaAs material used. The arrows indicate the position of the As and Ga signals, the latter referring to a surface layer of about 50 Å thick. For more details, in Fig. 8 we report two series of XPS spectra corresponding to samples examined before [Fig. 8(a)] and after [Fig. 8(b)] the chemical deoxidization procedure. The areas of the peaks related to each component were used to evaluate the As/Ga ratio.

For a better understanding of the mechanisms involved in LPPLA, we made a systematic study of the dependence of the As/Ga ratio on the annealing conditions. In Fig. 9, we have plotted the ratio of 3*d* peaks normalized to the corresponding FES coefficients for oxidized (curve *a*) and deoxidized (curve *b*) samples. The experimental points *A*1 and *B*1

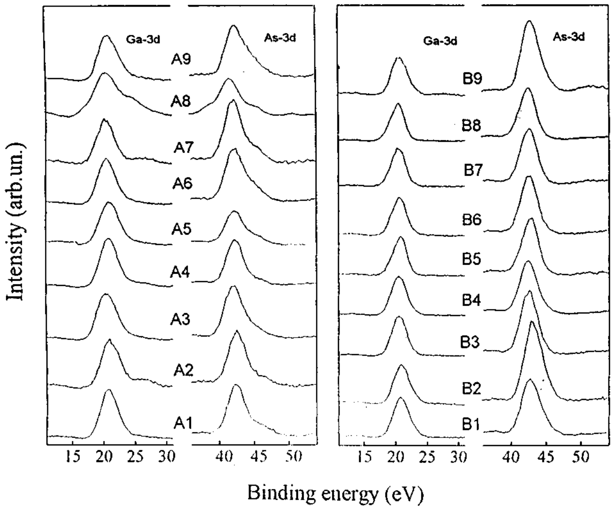

FIG. 8. Comparison between 3*d* core levels of Ga and As in GaAs samples: virgin (1), as-implanted (2), and laser annealed with 30 pulses of 4.5 MW/cm^2 (3); and 5 (4), 5.5 (5), 6 (6), 6.5 (7), 7 (8), and 7.5 MW/cm^2 (9), respectively, before (*A*) and after (*B*) deoxidization treatment.

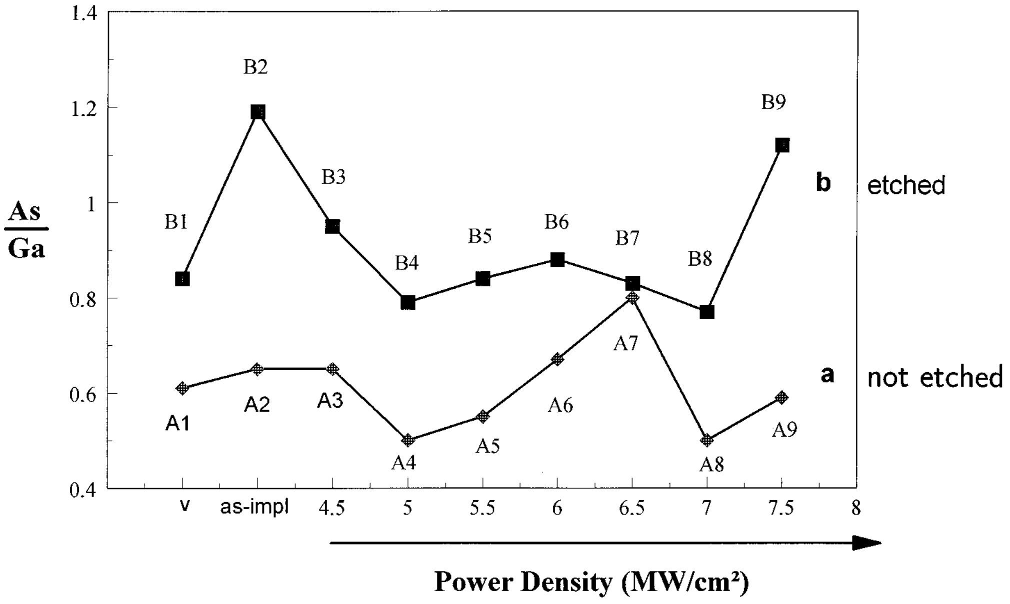

FIG. 9. Experimental As/Ga surface ratio as a function of the irradiation conditions for a GaAs sample before (*A*) and after deoxidization (*B*).

refer to virgin samples, and one can consider the value corresponding to *B*1 as a standard for the As/Ga concentration ratio at a clean surface of the substrate. The lower value of the oxidized virgin sample, corresponding to point *A*1, can be attributed to the presence of native oxides with oxygen bound preferentially to the Ga component (Ga_2O_3, Ga_2O_5) (Refs. 30 and 31) (in the related XPS spectrum the O signal is very strong indeed). During the deoxidization, the Ga atoms taking part in the oxide molecules are loosed in the chemical bath, so that the As/Ga ratio reaches a higher value, *B*1 (Fig. 9).

The XPS spectra taken after ion implantation reveal that, on the oxidized surface (see *A*2 in Fig. 9), the As/Ga ratio remains substantially unchanged while an As excess on the deoxidized surface is present (*B*2). This fact can be attributed to the intense formation of Ga oxides at the disordered surface layers of GaAs, which occurs when the specimen is exposed, after the implantation, to air at room temperature. Assuming that the ion-induced surface disorder enhances the oxygen adsorption, the thickness of the material with possible formation of Ga oxides is increased. The successive etching dilutes the Ga oxides leaving the surface layer enriched with As with a consequent increase of the As/Ga ratio (*B*2). In all cases the thickness of the surface oxide is small compared to that of the implanted layer, as confirmed by the ρ sheet resistivity measurements presented below.

Before further discussing the behavior of the curves presented in Fig. 9, it is worth noting that all the reported values are obtained by irradiating the samples, with different laser doses, starting from the same initial condition *B*2. As a consequence, the first laser pulse always impinges on an As-rich GaAs surface.

The LPPLA treatment carried out at 4.5 MW/cm^2 (*A*3 and *B*3) induces an initial in-depth diffusion of the As atoms with a consequent decrease of the surface As/Ga ratio toward the characteristic virgin value (*B*1). This fact, compared also with the results obtained by other analytical techniques, can be interpreted as an indication that a lattice reconstruction is beginning (*B*3).

At 5 MW/cm^2 (*A*4, and *B*4) and 5.5 MW/cm^2 (*A*5 and *B*5) the surface concentration ratio (points *B*4 and *B*5) becomes almost the same (within the experimental error) as that for the virgin sample (*B*1). One can possibly conclude that all crystal lattice positions have been occupied, and that the stoichiometric recovery is nearly complete. When the irradiation power density rises up to 6 MW/cm^2 (*A*6 and *B*6), the As oxides at the surface (e.g., As_2O_3) seem to increase, as one can see from *A*6, while the As/Ga ratio on the deoxidized samples remains about unchanged. This situation supports the idea that at this power density the irradiation provokes a weakening of the As-Ga bonds, so that the surface As atoms may be oxidized in a thermodynamically stable form. Furthermore, at 6.5 MW/cm^2 (*A*7 and *B*7) the As/Ga concentration ratio in the oxidized sample peaks to about the same value as that of the deoxidized specimen. One could conclude from here that under laser action the As-Ga bonds are weakened enough to oxidize all surface As atoms, but not to release them. This corresponds to the As sublimation limit, i.e., the power density response temperature above which the alteration in the stoichiometry of the surface layers becomes substantial, as illustrated by (*A*8) and (*B*8).

Finally, when the irradiation power density is set at 7.5 MW/cm^2, the As/Ga concentration ratio at the etched surface (*B*9) increases strongly due to a heating above the As sublimation temperature in a thicker layer of the material and an outdiffusion of the As interstitial atoms;[32] the latter are accumulated in a region just below the oxidized surface acting as a capping layer. The increase from *A*8 and *A*9, being lower than the corresponding increment at the deoxidized surface from *B*8 to *B*9, can be interpreted as a capping effect resulting from the surface oxide formed by the laser itself. As a consequence the arsenic component in the surface oxides increases. Due to the high-energy density deposited at the surface, in this case all laser pulses other than the first ones contribute to exceeding the sublimation temperature limit in the surface layers; in fact, the laser energy absorbed at the oxide is no longer sufficient to protect the bulk material from overcoming this limit.

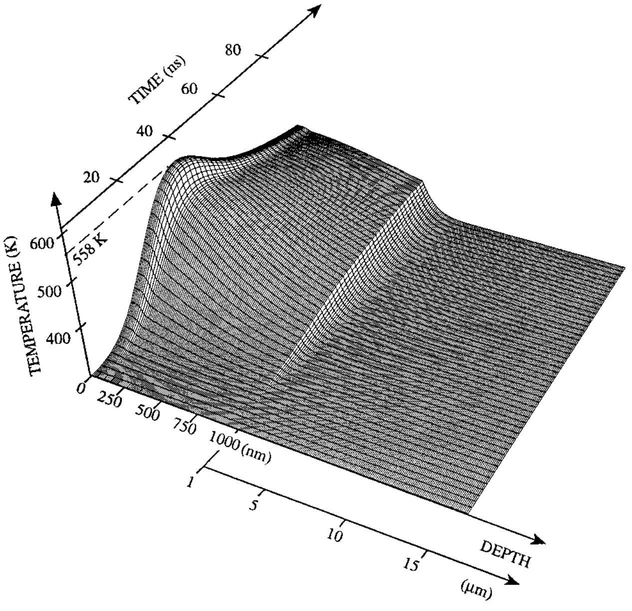

FIG. 10. Numerical calculations of the temperature distribution as a function of the depth and time for an InP sample irradiated with a power density of 6 MW/cm^2.

The slight mismatch between the calculated value of the upper power-density limit (6 MW/cm^2), and the XPS experimental results showing a limit of about 6.5 MW/cm^2, is probably due to the assumption made in the theoretical model which neglects the presence of a surface oxide and considers the laser energy instantaneously transferred to the lattice.

B. InP case

The temperature behavior obtained with the numerical calculation of InP treated by LPPLA at $P_0 = 6$ MW/cm^2 is illustrated in Fig. 10. The critical temperature of the compound, T_c, is considered as equal to 573 K, assuming that above T_c the losses of P become substantial.[6]

1. RHEED analysis

The relevant RHEED patterns (Fig. 11) show that the LPPLA treatment is able to recover the lattice order compared to that of the implanted sample, with negligible additional disorder due to the laser processing itself. One can deduce from these observations that the dissociation temperature in these conditions is not reached, in agreement with the calculations. Indeed, the temperature behavior shows (Fig. 10) that the maximum surface temperature $T_M = 558$ K is reached about 44 ns after the beginning of the laser pulse. The T_M value is below T_c, so that the laser irradiation supplies energy to the lattice without any further damaging of the crystal. Conversely, the laser-induced damage appears clearly when the irradiation energy density rises above the dissociation limit, i.e., when T_M exceeds the critical temperature.

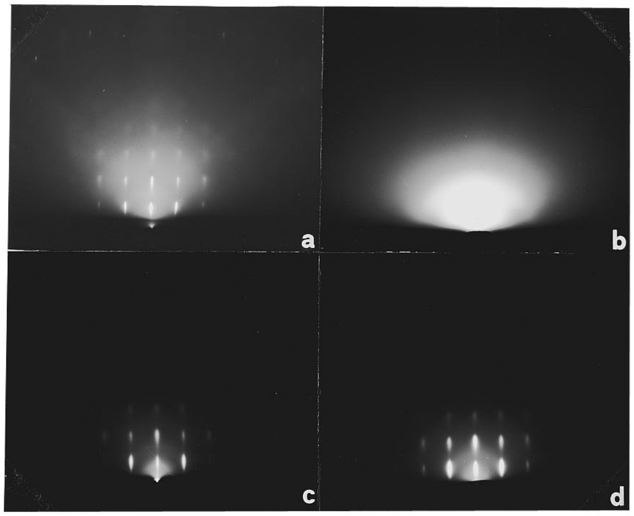

FIG. 11. Diffraction patterns along the ⟨001⟩ azimuthal direction of InP samples: virgin (a), implanted (b), and laser annealed with five pulses of power densities of 6 (c), and 7 MW/cm^2 (d).

2. RBS analysis

The structural recovery of InP induced by LPPLA was also analyzed by using Rutherford backscattering spectrometry (RBS) carried out in the channeling mode. In Fig. 12 we report these spectra (showing the In peak only) for three different samples: virgin (2), as-implanted (1), and treated by LPPLA (3) with 15 pulses at 6.5 MW/cm^2 each. The spectra present the distribution of the damage, i.e., the background of each spectrum is already subtracted. The irradiation conditions are chosen within the efficient energy window of the LPPLA technique.

As expected, the spectrum of the as-implanted sample gives the highest yield (Fig. 12, curve 1) resulting from the ion-beam-induced structural disorder. Conversely, the RBS spectrum for the LPPLA sample (Fig. 12, curve 3) shows the lowest yield. One can note that as a consequence of the laser treatment the surface damage is even smaller than that of the virgin specimen. This behavior supports the idea that in the case of well-prepared semiconductor wafers the LPPLA processing also removes the shallow surface disorder induced by the final polishing procedure.[11]

The RHEED analysis was not able to detect this difference due to its low sensitivity (since the diffraction patterns

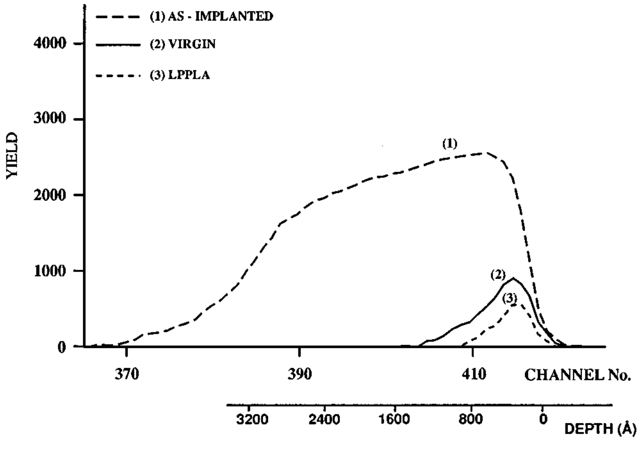

FIG. 12. Aligned RBS spectra for InP samples: as-implanted (1), virgin (2), and implanted pulse LPPLA (3) with 15 pulses of 6.5 MW/cm^2 each.

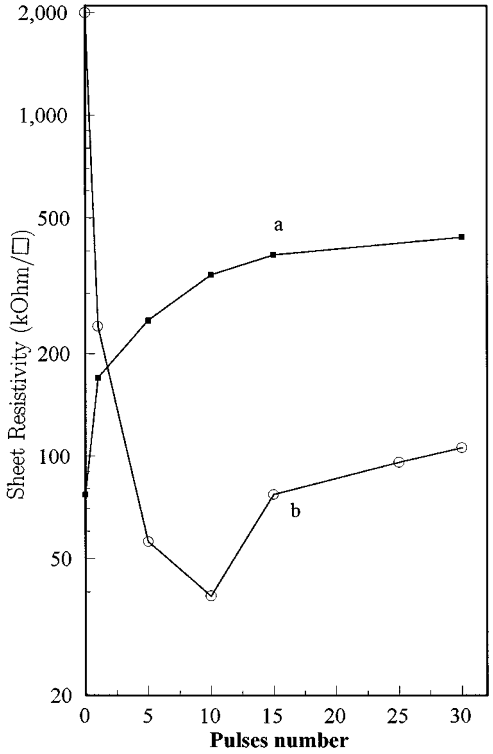

FIG. 13. Sheet resistivity of GaAs- (a) and InP- (b) irradiated samples as a function of the pulse number. The power density was 5 MW/cm^2 for the GaAs sample, and 6.5 MW/cm^2 for InP.

are mainly influenced by atoms occupying the lattice sites). Conversely, the RBS channeling technique is sensitive to a small number of defects altering the crystal channel continuity and/or regularity.

3. XPS analysis

The results of the XPS measurements for virgin, as-implanted, implanted, and laser-treated InP samples will be published elsewhere.[33] The dependence of the P/In surface concentration ratio on the irradiation conditions were investigated showing a behavior analogous to that for GaAs. In fact the P/In ratio, drastically altered for the implanted sample, was demonstrated to decrease, at increasing irradiation power density, down to values typical of the virgin InP obtained with $P_0 = 6.5$ MW/cm^2.

4. Electrical measurements

In addition, we have studied the resistivity behavior of laser-annealed specimens depending on different parameters such as the total laser dose, number of laser pulses, etc. We have reported earlier similar study for the GaAs case,[34] showing that a good electrical carriers activation can be achieved only if a thermal treatment at relatively low temperature (580 °C) is combined with LPPLA. Here we present only the results for the InP case concerning the dependence of the sheet resistivity on the number of laser pulses [Fig. 13(b)], and compare the behavior with that of GaAs. In the latter case[34] the increase in the number of laser pulses at LPPLA led to a recovery of the structural disorder induced by ion implantation, and to an increase of the sheet resistivity, probably due to a reduction of the defects density in the gap.[35] In InP [Fig. 13(b)] this effect on the sheet resistivity seems to be opposite, i.e., increasing the number of laser pulses N results in a drastic fall of ρ_s by about two orders of magnitude (from 2 MΩ/□ to 20 kΩ/□ when N_p increases from 0 to 10). Since, according to RHEED data, the structural reordering agrees well with the ρ_s behavior, one can therefore assume an increase in the carrier densities and/or their mobility with N_p.

The interpretation of the ρ_s behavior as an immediate enhancement of the carrier mobility seems to be in contrast with the increase of ρ_s for $N \geqslant 15$ [Fig. 13(b)] if one does not consider the role of the oxide formation. After the first few laser pulses, quite a thick oxide layer is formed on the sample surface (as revealed by RHEED) which begins to decrease the penetration of the laser energy toward the bulk. The laser pulses coming later induce the adsorption of the oxygen atoms by the surface, thus increasing the sheet resistivity again. In other words, the increase of ρ_s which can be ascribed to the presence of surface oxides does not rule out a cumulative effect of LPPLA in the structural reordering.

The important conclusion from the LPPLA processing of InP samples in air is that the laser irradiation itself, producing a thick oxide layer, at some stage stops and prevents the further effect of LPPLA. In order to gain the full advantage of the cumulative effect of laser pulses in LPPLA on the sheet resistivity of InP, one has to complete all measurements in a controlled inert (e.g., Ar) atmosphere. Such control experiments are now under way.

The upper limit for LPPLA is obtained by irradiating the InP samples with a power density of $P_0 = 7$ MW/cm^2. Similar to the case for GaAs, the distortion of the stoichiometry in the implanted layer is indicated by increase of the spot size and by spreading of the Kikuchi lines in the diffraction patterns [see Fig. 11(d)]. These observations are in agreement with the numerical predictions for GaAs- and InP-implanted samples irradiated with 6 and 7 MW/cm^2, respectively, as reported in Figs. 14 and 15 where the temperature can apparently exceed the critical sublimation values for both As and P atoms.

Furthermore, in order to illustrate the temperature gradient fields inside the specimen (which in the authors' opinion are responsible for the defects migration), we have calculated the space distribution of the temperature gradient as a first derivative of the temperature (plotted in Fig. 14) with respect to the in-depth coordinate. One can find that maximum damage is observed in the region where the (negative) temperature depth gradient has a minimum (i.e., maximum absolute value), this value being responsible for the migration of point defects toward the undamaged crystal. The calculated temperature space gradient versus time and in-depth coordinates is shown as a density plot in Fig. 16, the lighter and darker zones corresponding, respectively, to higher and lower absolute values of this gradient. The lighter zones can be considered as space-unstable regions where the laser energy is absorbed uniformly in the vicinity of each point only. The maximum absolute value of the temperature depth gradient is of the order of 10^6 K/cm.

In Fig. 17 we present a similar density distribution of the temperature time gradient (calculated as absolute values of the first derivative of the temperature from Fig. 14 with respect to time) vs time and depth. As before, the lighter and

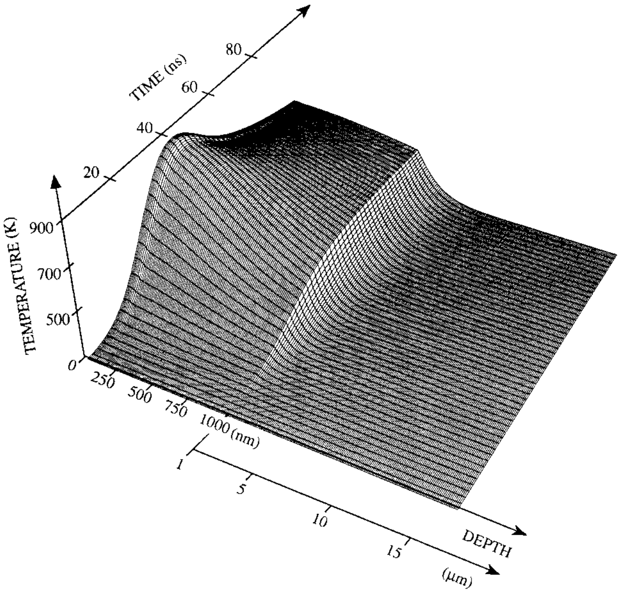

FIG. 14. Numerical calculations of the temperature distribution as a function of the depth and time for a GaAs sample irradiated with a power density of 6 MW/cm^2 (Ref. 13).

darker zones correspond, respectively, to higher and lower absolute values of the gradient. It may be worth noting that the existence of this gradient is not in conflict with the initial assumption that the energy is transferred instantaneously toward the lattice. The time gradient of the temperature results from the Gaussian-like shape of the laser pulse vs time, and therefore of the energy transfer to the crystal lattice. In other words, the plot in Fig. 16 indicates time-space regions with an energy-transfer rate so intense (with respect to the heat propagation) that quite an unstable equilibrium state vs time at each point originates.[35] In this sense the regions character-

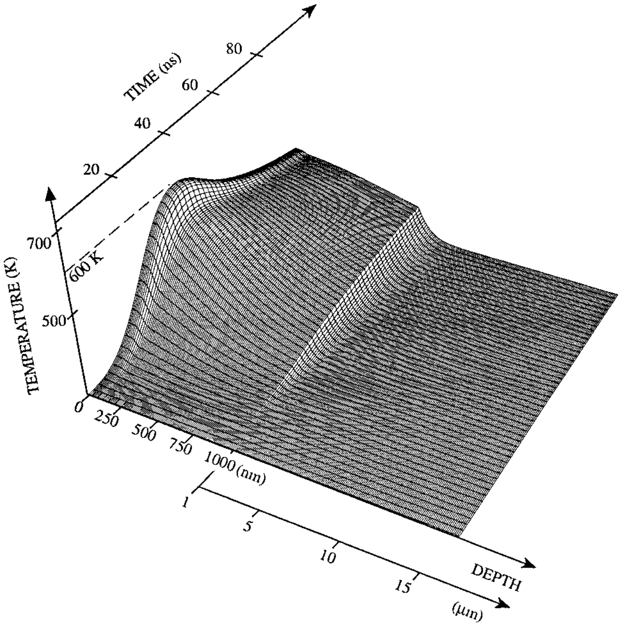

FIG. 15. Temperature surface, calculated by the numerical model, as a function of the depth and time for an InP sample irradiated with an energy of 7 MW/cm^2.

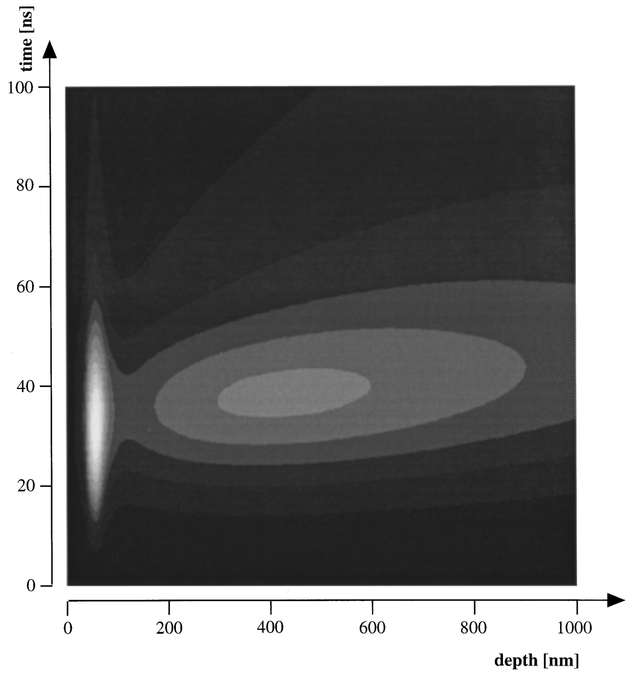

FIG. 16. Density plot of the space-temperature gradients, in absolute value, of a GaAs-irradiated sample with an energy density of 5 MW/cm^2 in dependence on the time and in-depth coordinates. The lighter and darker zones correspond, respectively, to higher and lower absolute values of the temperature space gradients.

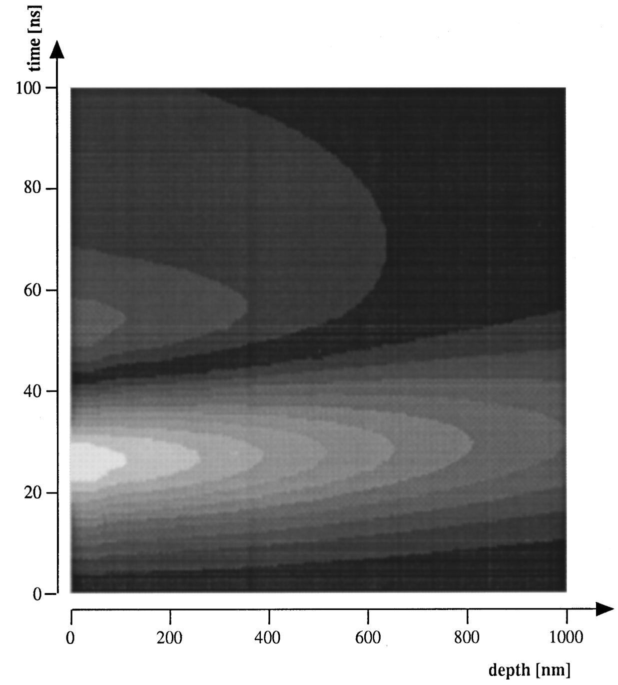

FIG. 17. Density plot of the time-temperature gradients, in absolute value, of a GaAs-irradiated sample with an energy density of 5 MW/cm^2 in dependence of the time and in-depth coordinates. The lighter and darker zones correspond, respectively, to higher and lower absolute values of the temperature time gradients.

ized with higher values of the temperature time gradient can be considered to be unstable in time. In our opinion such a condition should be necessary in order to achieve solid-phase epitaxial regrowth based on the migration of point defects set free under the action of laser-induced space thermal gradients. As a consequence, matching the time-unstable regions with the space-unstable areas, one can possibly evaluate the time-space coordinates of interest to the solid-phase epitaxial regrowth.

The role played by the laser-induced thermal gradients could be fundamental in determining the lower limit of the power density window where the low-power pulsed-laser-induced epitaxial regrowth takes place. In fact a solid-phase epitaxial regrowth can be obtained only if the irradiation power density delivered on the sample induces space and time gradients strong enough to produce nonequilibrium zones.

The last statement is, indeed, one of the two following fundamental hypotheses necessary to assume for a qualitative explanation of the LPPLA.

(1) The laser energy is absorbed mainly by weakly bonded electrons, located at the point defects (e.g., interstitials) in an unstable equilibrium.

(2) During the laser-energy absorption these point defects, in a pseudofree condition, can migrate through the potential barriers in the solid matrix, driven by the local thermal gradients. These gradients are due to the difference in the absorption coefficient of the residual crystalline isles. The presence of the latter near the surface of low-dose ion-implanted substrate is clearly observed by high-resolution transmission electron microscopy (HRTEM) (see, e.g., Ref. 25). At high implantation dose, when crystalline isles disappear, the transversal thermal gradients are correspondingly absent, and no efficient LPPLA processing was found. In order to increase the annealing effect, it is necessary to facilitate the interstitials vacancies annihilation, and destroy the point-defect clusters: successive superimposed laser pulses are especially needed for that purpose.

V. CONCLUSIONS

In the present paper we have outlined, first, mathematical method of calculating the distribution of temperature as a function of both the relaxation time and the depth of implanted GaAs and InP samples during their LPPLA treatment. Then, using a suitable optical experimental system, we have carried out LPPLA experiments and then, on the treated samples, investigations with several complementary techniques to verify the calculated temperature rise during the laser irradiation and thus to achieve an annealing of the implanted materials without appreciable stoichiometric changes.

The results obtained for both GaAs and InP show good agreement with the theory. In particular, the data reported for the GaAs case show that just in the energy window where the annealing occurs (points *B*4–*B*7 of curve *b* in Fig. 9) the Ga/As ratio remains substantially constant. The electrical measurements proved the capacity and the limits of the LPPLA technique to change the resistivity of the samples, as well as the difference between the GaAs and InP specimens. The results revealed that much higher carrier mobility values are obtained by LPPLA of InP than for GaAs in the same conditions. Another important difference is that the formation of laser-induced oxides on InP puts a strong limitation on the application of the LPPLA technique in air. This oxidation leads to a fundamental decision that all the LPPLA experiments on InP should be completed in a vacuum chamber: by avoiding the formation of oxides, one can increase the number of the applied laser pulses and also the total energy deposited at the surface.

The data analysis in the previous sections confirms the ability of LPPLA to recover the lattice order in III-V compound semiconductors via laser-induced epitaxial regrowth in a solid phase not only for GaAs (which was already reported earlier) but also for InP. In both cases the upper limit of the LPPLA window can be related to the laser-induced change of the stoichiometric ratio, while the lower limit probably takes its origin from the existence of an energy threshold below which the obtained thermal gradients are not sufficient to make effective the migration of defects across the matrix potential barriers.

It should be noted that within the model assuming inhomogeneity, the maximum of the space-gradient distribution is situated just in the region of the maximum damage produced by the implantation. The high absolute values of these gradients can be considered as responsible of the nonequilibrium condition where an epitaxial regrowth of the solid phase arises.

On the basis of the discussed experimental results, some ideas about the mechanisms involved in LPPLA-induced solid-phase epitaxial regrowth have been proposed. At this purpose, it is worth to underline that they are not yet completely understood, and that a comprehensive dynamical model of LPPLA is still to be achieved.

In conclusion we may say that the LPPLA technique is efficient in recovering the structural order of ion-implanted substrates of III-V semiconductor compounds when the power density of the laser irradiation is low enough to avoid reaching the compound dissociation temperature at the specimen surface. If LPPLA is applied at a power density exceeding this limit, the treatment will cause a cumulative loss of the more volatile element, so that the stoichiometry of the compound will be altered.

ACKNOWLEDGMENTS

The authors wish to thank Professor D. Karpuzov (Institute of Electronics, Bulgarian Academy of Sciences, Sofia) for his fundamental help in discussing all the matter, and for his critical review of the paper.

APPENDIX A

Here we report an analytical approach based on the Green-function method, and used to evaluate the temperature distribution as a function of the time and the depth inside the irradiated specimens.[36] For these calculations we assumed a two-layer model with thermal, optical, and implantation parameters reported in Tables I–III.

APPENDIX B

Here we describe the numerical method used to evaluate the temperature distribution as a function of the time and depth inside the irradiated specimens considering all the nonlinear thermal parameters (Table IV) and the model already described in the text to take into account the inhomogeneity of the ion-implanted specimen.[36] The applied algorithm comes from a modification of the Crank-Nicolson scheme in order to ensure stability and convergence.

---

[1] M. K. Brodsky, Sci. Am. **260**, 52 (1990).

[2] D. V. Morgan and F. H. Eisen, in *Gallium Arsenide: Materials, Devices and Circuits*, edited by M. J. Howes and D. V. Morgan (Wiley, New York, 1985), p. 161.

[3] B. J. Sealy, R. Bensalem, and K. K. Patel, Nucl. Instrum. Methods Phys. Res. Sect. B **6**, 325 (1985).

[4] T. Hiramoto, T. Saito, and T. Ikoma, Jpn. J. Appl. Phys. **24**, L193 (1985).

[5] C. T. Foxon, J. A. Harvey, and B. A. Joyce, J. Phys. Chem. Solids **34**, 1693 (1973).

[6] L. G. Van Uihtert, P. K. Gallagher, S. Singh, and G. J. Zydzik, J. Vac. Sci. Technol. B **3**, 825 (1983).

[7] S. S. Kular, B. J. Sealy, K. G. Stephens, D. Sadana, and G. R. Booker, Solid-State Electron. **23**, 831 (1980).

[8] S. J. Pearton, K. D. Cummings, and G. P. Vella-Coleiro, J. Electrochem. Soc. **132**, 2743 (1985).

[9] N. J. Barrett and B. J. Sealy, Electron. Lett. **20**, 175 (1984).

[10] G. Vitali, M. Bertolotti, G. Foti, and E. Rimini, Phys. Lett. **63A**, 351 (1977).

[11] G. Vitali, M. Rossi, D. Karpuzov, H. Budinov, and M. Kalitzova, J. Appl. Phys. **69**, 3882 (1991).

[12] G. Vitali, Jpn. J. Appl. Phys. **31**, 2049 (1992).

[13] G. Zollo, L. Palumbo, M. Rossi, and G. Vitali, Appl. Phys. A **56**, 409 (1993).

[14] G. Vitali, Italy Patent No. 47882-A/84-03.16.1984 (pending); Germany Patent No. P-3509421.4-03.15.1985. (pending)

[15] E. A. Kraut, R. W. Grant, J. R. Waldorp, and S. P. Kowalczyk, Phys. Rev. B **28**, 1965 (1983).

[16] I. M. Band, Yu. I. Kharitonov, and M. B. Trzhaskovskaya, At. Data Nucl. Data Tables **23**, 443 (1979).

[17] G. Zollo, Ph.D. thesis, Università ''La Sapienza,'' Roma, 1996.

[18] A. N. Tichonov, A. A. Samarskij, and B. Budak, *Problem Della Fisica Matematica*, translated from *Sbornik Zadak po Matematiceskoj Fizike* (MIR, Moscow, 1982).

[19] P. Morse and H. Feshbach, *Methods of Theoretical Physics* (McGraw-Hill, New York, 1953).

[20] H. S. Carlslaw and J. C. Jaeger, *Heat Conduction in Solids* (Oxford University Press, London, 1959).

[21] J. C. Brice, *Properties of Gallium Arsenide* (Gresham, London, 1986).

[22] J. C. Brice, *Properties of Indium Phosphide* (Gresham, London, 1991).

[23] M. R. Madison and T. W. McDaniel, J. Appl. Phys. **66**, 12 (1989).

[24] G. Vitali, G. Consalvi, C. Pizzuto, M. Rossi, and G. Zollo, Radiat. Eff. **132**, 196 (1994).

[25] M. Kalitzova, N. Pashov, G. Vitali, and M. Rossi, in *Processing and Characterization of Materials Using Ion Beams*, edited by L. E. Rehn, V. Greene, and F. A. Smidt, MRS Symposia Proceedings No. 128 (Materials Research Society, Pittsburgh, 1989), p. 683.

[26] W. S. Ames, *Numerical Methods for Partial Differential Equations* (Academic, New York, 1977).

[27] A. N. Tichonov and A. A. Samarskij, *Equazioni della Fisica Matematica*, translated from *Uravnenija Matematiceskoi Fiziki* (MIR Moscow, 1981).

[28] A. R Mitchell and D. Driffits, *The Finite Difference Methods in Partial Differential Equations* (Wiley, New York, 1980).

[29] J. Crank, *The Mathematics of Diffusion*, 2nd ed. (Oxford University Press, London, 1990).

[30] G. P. Schwartz, Thin Solid Films **103**, 3 (1982).

[31] M. Hall, M. F. Rau, and J. W. Evans, J. Electrochem. Soc. **133**, 1934 (1986).

[32] G. Vitali, M. Rossi, D. Karpuzov, H. Budinov, M. Kalitzova, and I. Katardjiev, Nucl. Instrum. Methods Phys. Res. Sect. B **59/60**, 1077 (1991).

[33] V. Krastev, Ts. Marinova, M. Kalitzova, G. Vitali, and C. Pizzuto (unpublished).

[34] G. Vitali, C. Pizzuto, M. Rossi, G. Zollo, D. Karpuzov, and M. Kalitzova, Jpn. J. Appl. Phys. **33**, 5 (1994).

[35] L. D. Laude, in *Interfaces Under Laser Irradiation*, Vol. 134 of *NATO Advanced Study Institute, Series E: Applied Sciences*, edited by L. D. Laude, and M. Wautelet (Plenum, New York, 1987).

[36] See AIP document no PAPS PRBMD-53-4757-6 for 6 pages of Appendix B. Order by PAPS number and journal reference from American Institute of Physics, Physics Auxiliary Publication Service, Carolyn Gehlbach, 500 Sunnyside Boulevard, Woodbury, New York 11797-2999. The price is $1.50 for each microfiche (98 pages) or $5.00 for photocopies of up to 30 pages, and $0.15 for each additional page over 30 pages. Airmail additional. Make checks payable to the American Institute of Physics.